Detection, visualization, quantification, and warning of pipeline corrosion using distributed fiber optic sensors

Xiao Tan [1], Liang Fan [2], Ying Huang [3], Yi Bao [1,*]

[1] Department of Civil, Environmental and Ocean Engineering, Stevens Institute of Technology, Hoboken, NJ 07030, United States

[2] Department of Civil and Environmental Engineering, Washington State University, Pullman, WA 99163, United States

[3] Department of Civil and Environmental Engineering, North Dakota State University, Fargo, ND 58105, United States

* Corresponding to Dr. Yi Bao: yi.bao@stevens.edu

Abstract

This paper presents a distributed monitoring approach to detect, visualize, quantify, and warn pipeline corrosion using a single-mode telecommunication-grade fiber optic cable. The fiber optic cable can be deployed on the external surface of a steel pipe and serves as a distributed sensor to measure the corrosion induced strain over the surface along the pipe based on optical frequency domain reflectometry, which can be used to identify pipeline corrosion. To validate this distributed pipeline corrosion monitoring approach, in laboratory, a steel pipe with deployed sensor was immersed in a sodium chloride solution (concentration: 3.5 wt.%) for accelerated corrosion test. The strain distributions were used to detect and map corrosion along the pipe. An analytical model was developed and presented to link the measured strains to the mass loss of pipe under corrosion. The effects of sensor package thickness, spatial resolution, and deployment pattern on assessment of corrosion were investigated systematically. A threshold-based warning method is proposed based on the unique monitored sensor data. This study is expected to greatly advance corrosion monitoring and effective management capabilities for safe operation of pipeline.

Keywords: Corrosion; Distributed fiber optic sensors (DFOS); Optical frequency domain reflectometry (OFDR); Pipeline; Structural health monitoring (SHM); Visualization

1. Introduction

Pipeline is an important asset used to transport energy products such as oil and gas. According to the Pipeline and Hazardous Materials Safety Administration (PHMSA), the energy transportation network of the U.S. had over 2.8 million miles of pipeline by 2020 [1]. Usually buried unground, pipeline is subject to many threats, such as ground motion, excavation, and corrosion, which may cause pipeline leakage and catastrophic consequences concerning public safety. Long length of pipeline increases the probability of anomaly and increases the difficulty of detecting and locating damages on pipelines. Among various anomalies, corrosion is one of the most important causes of pipeline degradation, which continuously reduces pipe wall thickness and may significantly accelerate occurrence of leakage [2]. According to PHMSA, corrosion was responsible for about 25% of the incidents of natural gas pipeline in the last 30 years [3, 4]. According to the U.S. National Association of Corrosion Engineers (NACE), pipeline corrosion was responsible for a financial burden of about $7 billion every year [5].

Protective coatings and cathodic protection are effective preservation methods that can delay protection, but corrosion still occurs and causes incidents [6]. Many effects can damage protective coating and expose pipeline to corrosion, such as excavation, soil stress, water and corrosive contaminants, and high operating stress. Once corrosion is developed to a certain level, it is difficult to repair the pipe. Thus, early detection and mitigation of pipeline corrosion are of great importance in practice for pipeline maintenance.

Traditional pipeline inspection methods include direct assessment [7], hydrostatic pressure test [8], and nondestructive evaluation (NDE) using In-line inspection (ILI). Direct assessment is a preventative inspection method that may identify anomalies before they cause any costly issue, but it involves four steps as pre-assessment, indirect inspections, direct examinations, and post assessment, which are time consuming and labor intensive [9]. Hydrostatic pressure test is a destructive method, which is costly and difficult to conduct. In-line inspection (ILI) using pipeline inspection robots, namely smart "pigs", has attracted interests [10]. A smart pig may incorporate various nondestructive evaluation (NDE) techniques, such as magnetic fields [11], eddy current [12], ultrasonic [13] and acoustics emission [14]. As the smart pig travels in and along a pipeline, multiple types of anomaly can be detected. However, limitations of ILI were identified in practices including that (1) ILI cannot provide real-time monitoring data because it is only performed periodically; (2) ILI interrupts the operation of pipeline, which compromises resiliency and may increase operation cost [9]; And (3) many pipelines are unpiggable for different reasons, such as the variation of pipe diameter, acute bend, insufficient operating pressure, and so on [15]. Therefore, other effective methods that can provide real-time monitoring using onsite sensors and do not interrupt pipeline operation are desired.

In the literature, various sensing technologies have been proposed for monitoring corrosion in and on pipelines. A family of popular methods are based on electrochemical measurement, such as assessment of potentiodynamic polarization [16-18], linear polarization resistance [19-21], electrochemical impedance [17, 22], and electrical resistance [23, 24]. These sensors can be deployed at different cross sections of pipeline for real-time or near real-time measurements. The traditional methods based on electrochemical measurement might identify the likelihood of corrosion but can hardly locate and quantify corrosion in real-life applications. Alternatively, temperature and strain sensors have been developed to relate these detected parameters to pipeline corrosion such thermocouples and vibrating wire temperature sensors [26, 27] and electrical resistance strain gauges and vibrating wire strain sensors [27, 28]. Since these sensors are usually point sensors, each of these sensors monitors a local spot of pipeline, and many sensors are needed to monitor different sections along pipeline for an effective monitoring system. In addition, sensor installation and operation are difficult and costly because many sensors and wires are installed, operated, and maintained over a long time. Besides, the measurement from electrical sensors could be subjected to electromagnetic interference and can be affected by many other variables, such as environmental variables (e.g., temperature, relative humidity) and pipeline parameters (e.g., coating material and thickness) [25].

In the meanwhile, fiber optic sensors are attracting increasing interests in pipeline industry [29]. Compared with traditional sensors, fiber optic sensors have advantages such as immunity to electromagnetic interference (EMI), high accuracy, small size, and desired physical and chemical stability [30-33]. Fiber optic sensors can be categorized into point and distributed sensors. Example point sensors include fiber Bragg grating (FBG) sensors [34] and interferometer sensors [35]. In a FBG sensor, Bragg gratings are inscribed using lasers through a sophisticated process, to make the optical fiber sensitive to measurands (e.g., temperature and strain) [31]. In an interferometer sensor, a cavity is fabricated in the optical fiber. Point sensors need to be carefully packaged to protect gratings or cavity. Similar as the point strain or temperature sensors, each point fiber optic sensor only monitors a local spot [36]. Although it is possible to connect multiple sensors in series to form a "quasi-distributed" sensor for measurements at multiple discrete spots [37], the cost associated with sensor preparation and operation can be increased.

Alternatively, fully distributed fiber optic sensors can be a good candidate for pipeline corrosion monitoring. Compared with point sensors, a distributed sensor utilizes a single fiber optic cable as the transmission line and a sensor with thousands of sensing points without sophisticated treatment. Distributed sensors have been proposed to assess different anomalies, such as leakage, corrosion, and so on [38-48]. For example, distributed temperature and strain sensors were deployed along pipes to measure temperature and strain distributions [38], which were then used to assess pipeline condition. Corrosion of pipeline could induce a dimension change, which could be measured by fiber optic sensors and used to assess pipeline corrosion [39-41]. Other methods for assessment of pipeline corrosion may involve measurement of chemicals or magnetic effects associated with corrosion [42-48]. A detailed literature review of sensors for monitoring pipeline corrosion is provided in reference [2], covering both traditional corrosion sensors and fiber optic sensors. A distributed fiber optic sensor can provide continuous measurement along a pipeline over a long distance (more than 100 km) [49-51].

In the previous research on distributed fiber optic corrosion sensors, the emphasis was mainly placed on feasibility of using distributed sensors to detect corrosion. Although the results showed a good promise, some challenges concerning real-life applications have been identified as below: (1) It is a challenge for pipeline engineers and stakeholders to understand and accurately interpret the unique sensor data measured from the distributed sensors in practices. Skilled sensor experts are needed to process and explain the sensor data, thus, increasing the operation cost of distributed sensors. (2) It is unclear how the corrosion condition of pipeline can be quantitatively evaluated using the data measured from the distributed sensors. In general, the distributed sensor data are associated with the severity of corrosion. However, there is lack of effective tools to quantify the relationship and generate warning for pipeline condition. (3) It is unknown how corrosion assessment using distributed sensors is affected by key parameters of the fiber optic cable, sensing parameters, and sensor deployment methods. These challenges hinder the potential of a wider application of distributed sensors for enhancing the capability of pipeline monitoring and improving the safety.

This paper presents a distributed fiber optic sensing method to detect, locate, visualize, and quantify corrosion of steel pipeline, and provide warning based on measurements from the distributed fiber optic sensors. Specifically, this paper has three main contributions including (1) the development of a distributed sensing method to detect, locate, and visualize corrosion of pipeline; (2) the development of a novel method to quantify corrosion and provide warning; and (3) investigation of the effects of important influencing factors on the assessment of pipeline corrosion. To validate the developed distributed fiber optic sensing system, steel pipes were prepared and instrumented with distributed sensors, and immersed in a sodium chloride solution (concentration: 3.5 wt.%) for accelerated corrosion tests. During the laboratory tests, strain distributions were measured from the distributed sensors based on optical frequency domain reflectometry (OFDR) [52], and mass loss of pipes was evaluated using a high-precision microbalance. An analytical model was developed and presented to correlate the measured strains with mass loss of pipes due to corrosion. The effects of fiber type, spatial resolution, and deployment pattern on corrosion assessment were also investigated. A threshold-based warning method was developed based on corrosion assessment data for real-time pipeline corrosion status alarm.

The remainder of the paper is then organized as follows: Section 2 introduces the sensing principle and calibration of distributed sensors. Section 3 introduces the experimental program. Section 4 presents and analyzes the tests results. Section 5 summarizes the findings from this study.

2. Sensing Principle

2.1. Fiber optic cables

Three types of single-mode fiber optic cables were investigated, including a bare fiber and two coated fibers, as depicted in Figs. 1 (a-c). The bare fiber as shown in Fig. 1 (a) had a glass core (diameter: 9 μm), a glass cladding (diameter: 125 μm), an inner coating (diameter: 190 μm), an outer coating (diameter: 242 μm). Light waves propagate along the glass optical fiber through total internal reflection at the core-cladding interface. The inner coating is a soft acrylic layer which protects the glass fiber from mechanical impact, and the outer coating is a stiff acrylic layer which protects the glass from abrasion and environmental exposure. To further enhance the mechanical strength and facilitates operation of the fiber in practice, two coated fibers are packaged with tight buffers as shown in Figs. 1 (b, c) as a measured diameter of 650 μm and 900 μm, respectively.

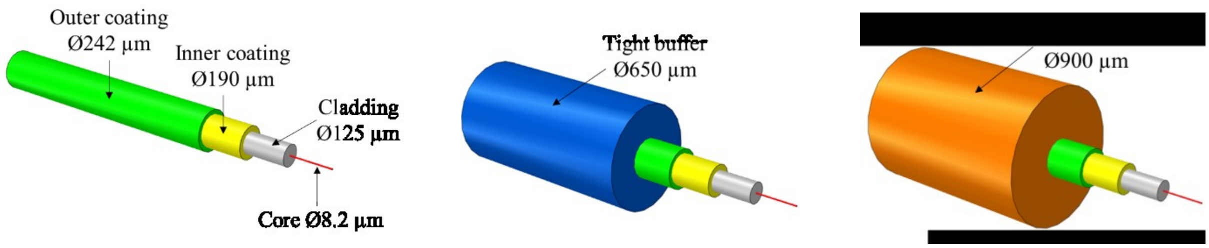

(a) (b) (c)

Fig. 1. Cross sections of fiber optic cables: (a) 242-μm-diameter bare fiber; (b) 650-μm-diameter coated fiber; and (c) 900-μm-diameter coated fiber.

2.2. Optical frequency domain reflectometry

Rayleigh scattering in an optical fiber describes an elastic scattering of transmitted light inside the glass core due to its irregular microstructure [53]. The irregularity can be generated during fiber fabrication, and the size of irregularity is comparable with the wavelength of the light wave. An example of irregular microstructure is the variation of the composition of glass, which results in variations in the refractive index and the density of the fiber core. The optical frequency domain reflectometry (OFDR) is used to measure strain and temperature based on Rayleigh scattering at two different states including the reference state and the perturbed state. In each state, a light wave is beamed into the optical fiber, generating Rayleigh scattering. The backscattered signal is measured from the optical fiber along fiber length. At each point of the fiber, the amplitude of the backscattered signal is plotted against the wavelength of the light. The amplitude versus wavelength data is converted into intensity versus frequency via Fast Fourier Transform. A cross-correlation operation is performed for the reference and the perturbed states, and a frequency shift can be identified for each spot along the optical fiber. The distance is determined by the travelling time of the backscattered light wave. In this study, a data acquisition system (model: Luna ODiSi 6) was used to perform the measurements. The manufacturer-specified measurement accuracy is 1 με for strain and 0.1 ºC for temperature [54]. More details about the principle of OFDR and applications can be found in references [55-57]. The frequency shift is associated with strain and temperature changes, as described in:

$$\frac{\Delta\lambda}{\lambda} = \frac{\Delta\nu}{\nu} = K_T T + K_\varepsilon \varepsilon \tag{1}$$

where λ and υ are the mean optical wavelength and frequency; and K_T and K_ε are the temperature and strain calibration constants, which were calibrated as -0.15 GHz/με and -1.46 GHz/°C [58], respectively. At a constant temperature, the spectral shift can be converted into strain along the optical fiber with a calibrated strain sensitivity coefficient. In the case that the temperature may vary, a temperature compensation optic cable will be needed to perform temperature compensation to ensure the accurate measurements of strains.

3. Experimental Program

3.1. Materials and specimen preparation

Fig. 2 shows the dimensions of the investigated pipes that were made using normal low-carbon steel and stainless steel, respectively. The materials of the investigates pipes are commonly used in pipelines for transmission of air, natural gas, oil, steam, and water following standards ASTM A733 [59] and ASTM A269 [60]. The outer diameter of pipes was 25.4 mm. The wall thickness was 3 mm. Each pipe measured 300 mm in length.

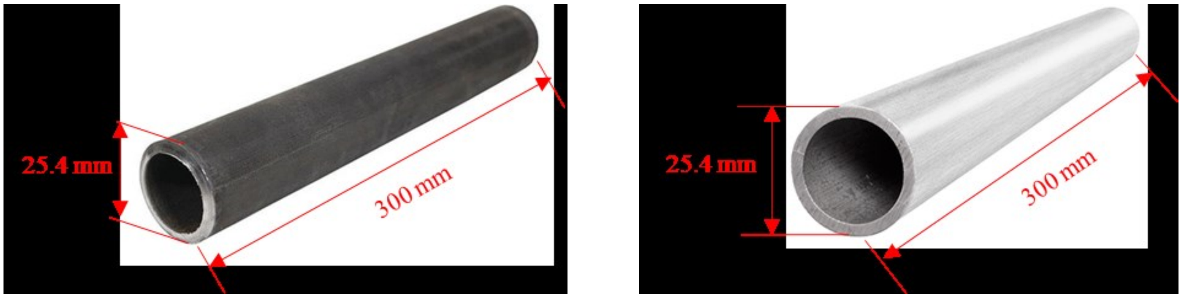

(a) (b)

Fig. 2. Depiction of the pipe specimens: (a) low-carbon steel pipe; and (b) stainless steel pipe.

A fiber optic cable was installed on the pipe after cleaning the rust on pipe surface in three steps. First, the fiber optic cable was attached to a pipe at discrete spots using tape which held the fiber in place. Second, the fiber optic cable was fixed on the pipe at discrete points using a fast-curing super glue. Third, the tape at discrete spots on the pipe was removed, and a two-part epoxy was applied along the length of fiber optic cable to ensure a reliable attachment of fiber and effective strain transfer between fiber and pipe. The epoxy only covered the fiber optic cable and the cable line on the pipe. Any epoxy that flowed away from the fiber optic cable was cleaned to avoid potential effect on pipe corrosion. Fig. 3 shows the deployment pattern of fiber optic cables. The fiber optic cable was installed on the pipe following a spiral pattern. Different spacings between adjacent rounds of spiral were investigated in this study to optimize the scheme of deployment.

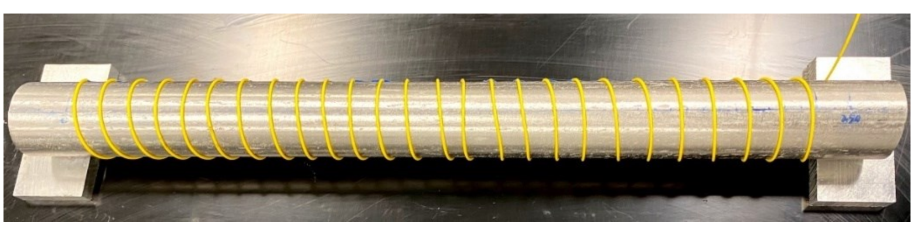

Fig. 3. Illustration of the installation of the distributed fiber optic sensors on a pipe specimen.

3.2. Investigated cases

A total of 14 different cases were investigated, as listed in Table 1. The pipe specimens were grouped into four categories, designated as P0 to P3. P0 was the control specimen made using stainless steel. P1 Group includes three specimens which were designed for low-carbon steel pipes used to investigate the effects of three different coating thicknesses of fiber optic cable (242 µm, 650 µm, and 900 µm). P2 Group includes one specimen that was designed to investigate the effect of five different measurement spatial resolutions of distributed sensor (0.65 mm, 1.3 mm, 2.6 mm, 10.4 mm, and 20.8 mm). P3 Group has five specimens to investigate five different deployment spacings (10 mm, 20 mm, 40 mm, 60 mm, and 80 mm).

Table 1. Investigated cases

Cases	Pipe group	Coating thickness (µm)	Spatial resolution (mm)	Spacing (mm)
1	P0	900	0.65	20
2	P1	242	0.65	20
3		650	0.65	20
4		900	0.65	20
5	P2	900	0.65	20
6		900	1.30	20
7		900	2.60	20
8		900	10.4	20
9		900	20.8	20
10	P3	242	0.65	10
11		242	0.65	20
12		242	0.65	40
13		242	0.65	60
14		242	0.65	80

3.3. Experimental set-up

When the adhesive was hardened after 24 hours (h), the pipes were put in a plastic container and immersed in a sodium chloride solution (concentration: 3.5% by mass) for corrosion tests at room temperature (25 ºC ± 2 ºC). Fig. 4 (a) shows the experimental set-up. The fiber optic cable was connected to the distributed sensing system for data acquisition as shown in Fig. 4 (c). Rayleigh scattering signals were measured and converted into strain distributions along the distributed sensor. Each of the measurements took about 20 seconds to 40 seconds. A distributed temperature sensor was deployed on the pipe for temperature compensation, which could eliminate the effect of temperature variation on the measurement of strain distributions. The pipes were supported by plastic blocks at the two ends to expose the bottom of the pipes to the sodium chloride solution as shown in Fig. 2 (b) as an example.

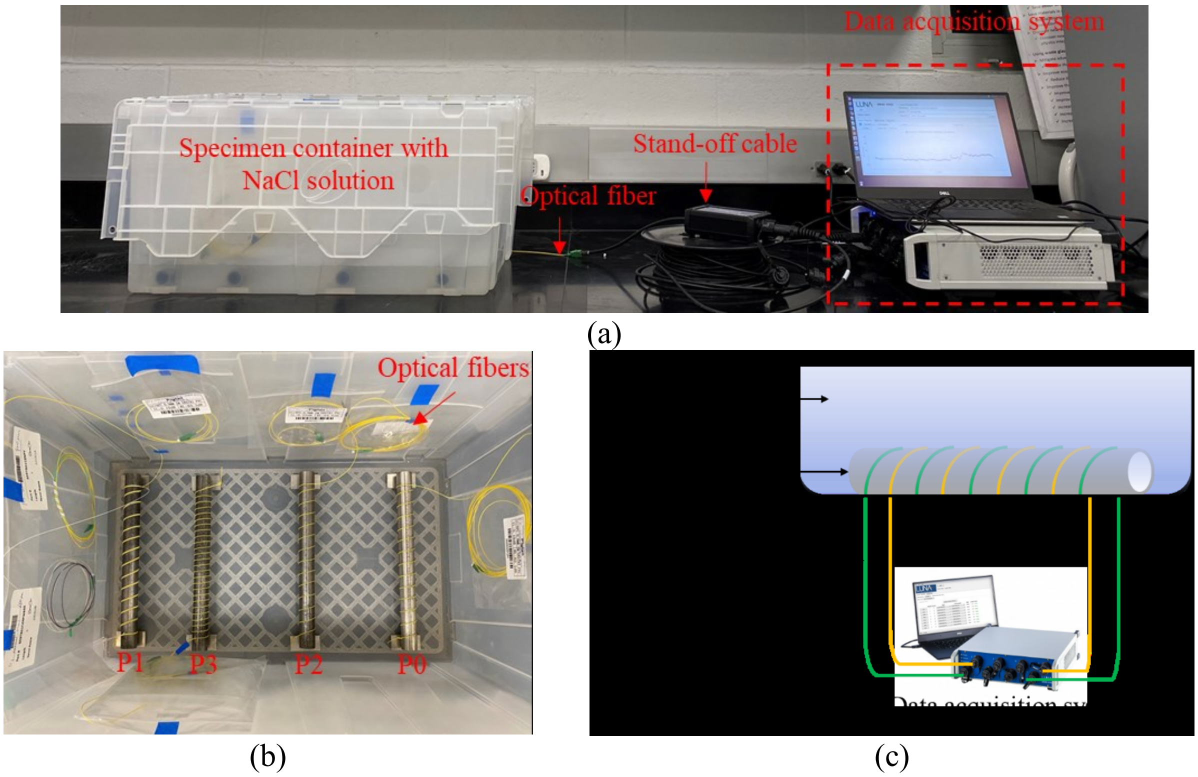

Fig. 4. Corrosion test of steel pipes: (a) test set-up; (b) specimens; and (c) illustration of a pipe instrumented with distributed sensors.

4. Experimental Results

4.1. Visual inspection

Fig. 5 shows an example of representative visual inspection results from one specimen in each testing group. No rust was observed on the control pipe (P0) made of stainless steel. Corrosion products were generated on the external surfaces of pipes in groups P1 to P3. As the immersion time increases, the thickness of rust was increased. Most rust was attached to the exterior surface of the pipes, and only a small volume of rust was transported off the pipes. Since the corrosion products are expansive and have low density compared with steel, the diameter of the corroded pipe was increased.

Fig. 5. Photo of four pipes immersed in the sodium chloride solution for different lengths of time.

4.2. Strain distributions

The increase of the pipe diameter caused strain changes in the distributed sensors on the pipes. Figs. 6 (a-j) show the corrosion-induced strain distributions measured from the distributed sensors at different immersion durations of 30h, 60h, 114h, 134h, 184h, 208h, 280h, 472h, 640h, 912h, and 1080h. The Y-axis represents tensile strain, and the X-axis represents the distance along the distributed sensor, with the zero distance at the connector of the data acquisition system. In each figure, the length range of the distributed sensor is selected to show the strain distributions within the length of fiber optic cable wrapped on the pipes. As shown in Fig. 6(a), for the control specimen, no obvious strain change was measured. Figs. 6(b) to 6(d) show the strain distributions measured from the distributed sensor deployed on the three P1 specimens using three types of fiber optic cable. For each specimen, obvious strain changes along the pipe were observed. Similarly, Fig. 6(e) shows the strain distributions measured from the distributed sensor deployed on a P2 specimen, and Figs. 6(f) to 6(j) show the strain distributions measured from the distributed sensor deployed on five P3 specimens. Nonuniform strain distributions along the pipes are observed because corrosion is uneven along the pipes. The uneven corrosion can be attributed to the different material defects and surface conditions along a pipe.

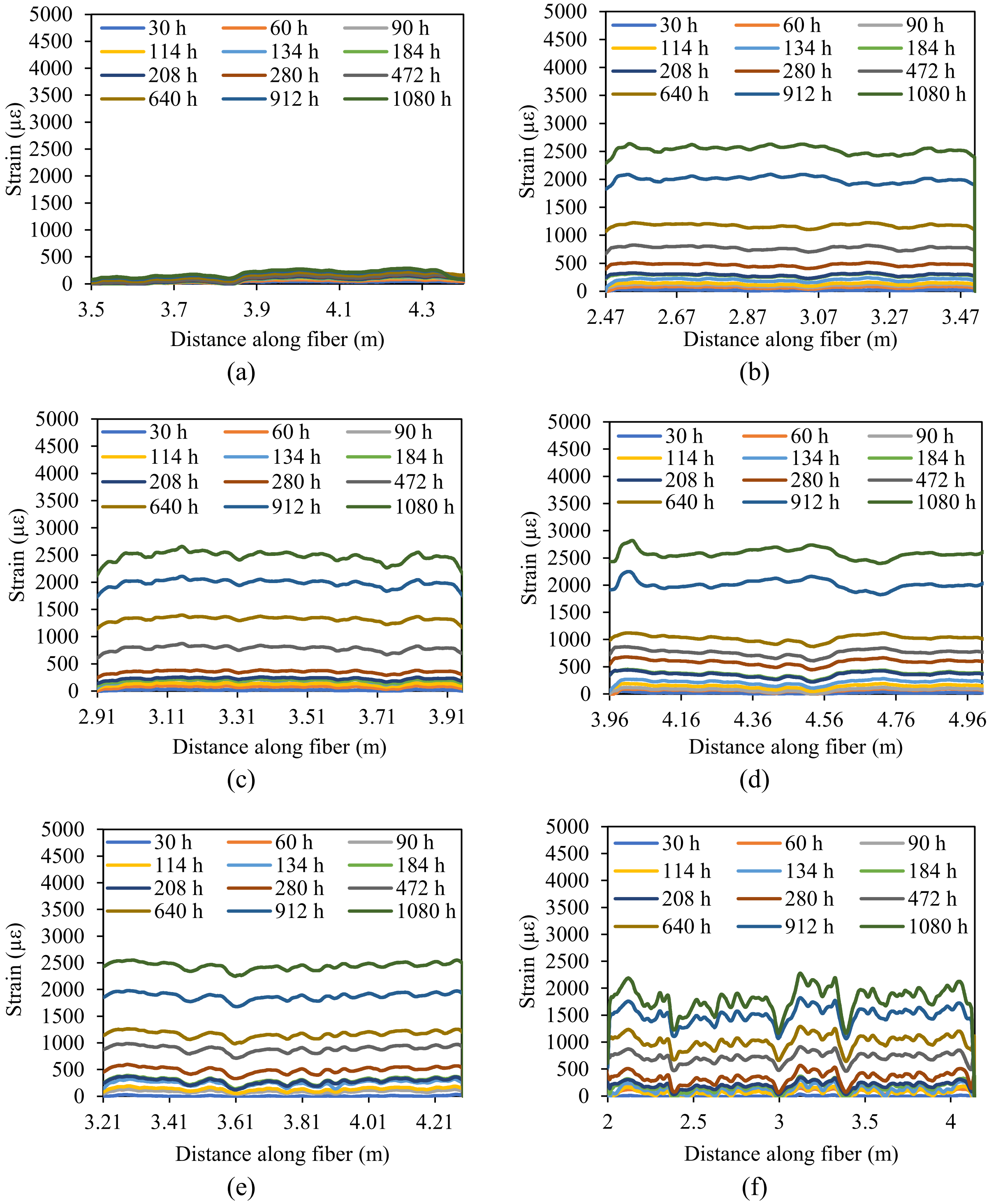

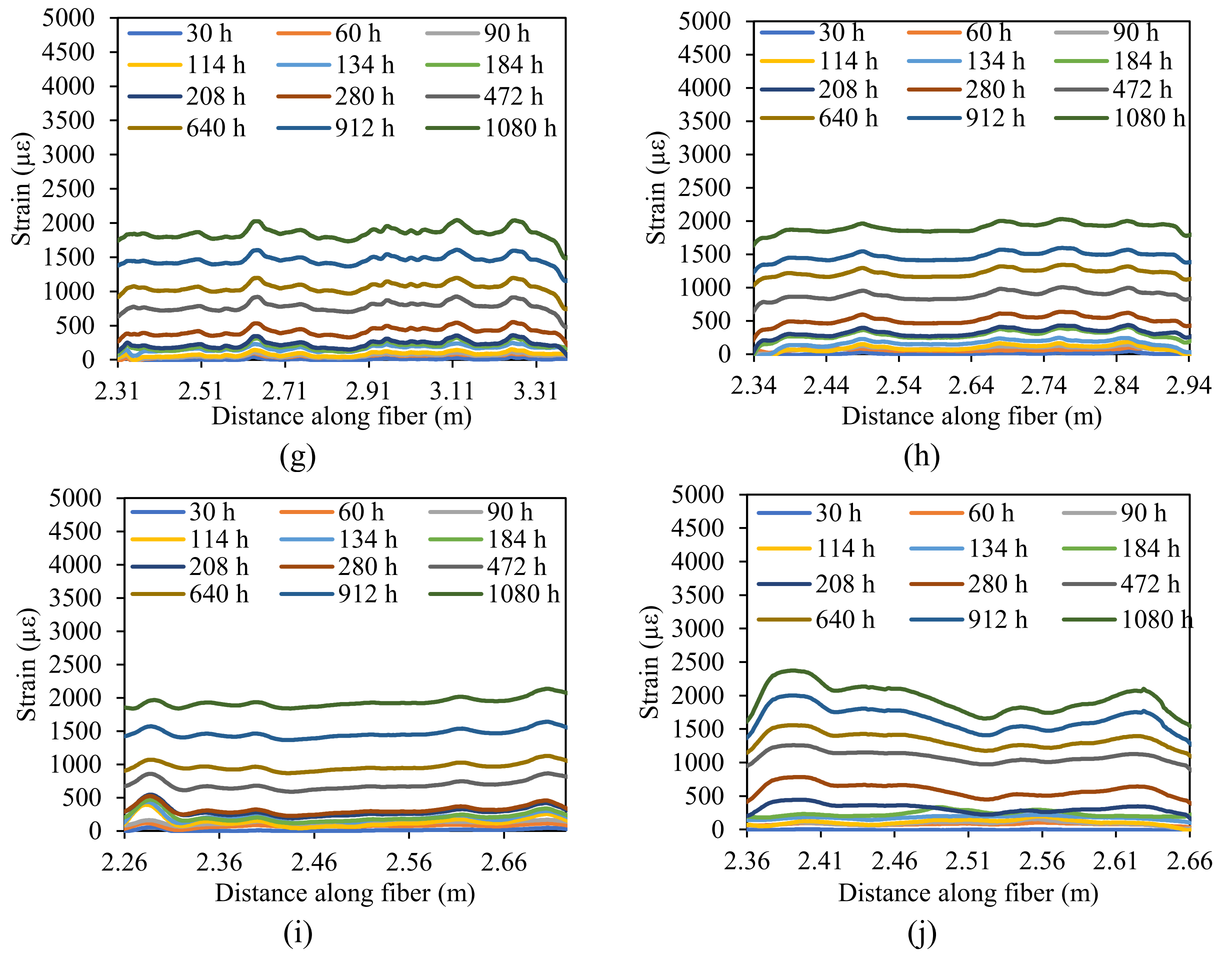

Fig. 6. Strain distributions measured from the distributed sensors along the pipe specimens: (a) P0; (b) P1-242 μm; (c) P1-650 μm; (d) P1-900 μm; (e) P2; (f) P3-10 mm; (g) P3-20 mm; (h) P3-40 mm; (i) P3-60 mm; (j) P3-80 mm.

4.3. Visualization

The expansion induced by corrosion of pipe was detected by the change of strains sensed by the distributed sensor. With the location of the distributed sensor installed on a pipe, the distance along the distributed sensor can be correlated with the position in the surface of the pipe. With the correlation, the strain distributions measured from the distributed sensor can be replotted through a coordinate transform, as illustrated in Fig. 7. The position of the distributed sensor attached to the surface of the pipe in the helix pattern is described in a polar coordinate system, which can be transformed into coordinated in a Cartesian coordinate system. Basically, the circular surface of the pipe is cut along the length, and the circumference is unfolded to a plane. The circumference of the pipe becomes the width of the plane, and the length of the pipe remains the length of the plane. Then, the strain distributions measured from the distributed sensor is plotted in the plane to show a two-dimensional contour of the strain, which can be used for visualization of corrosion condition in real time. The data between adjacent paths of fiber optic cable were obtained through linear interpolation. The different paths of the distributed sensor show the variation of strains.

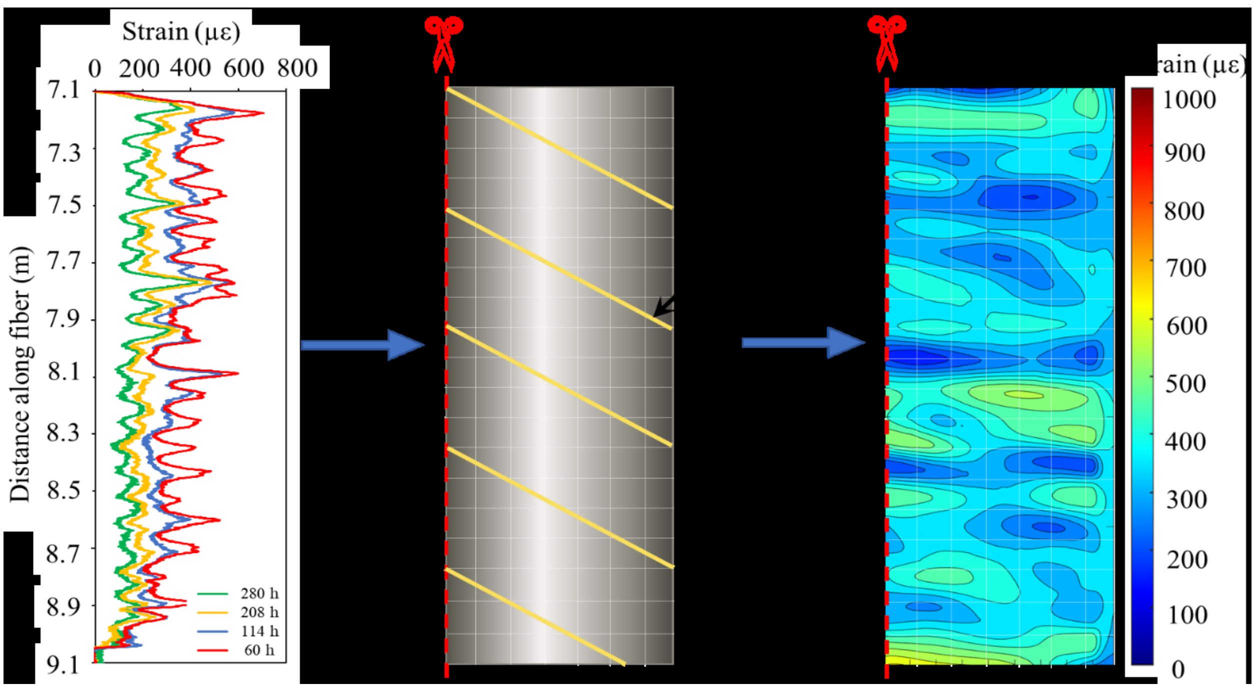

Fig. 7. Method of mapping strain distribution on a pipe for visualization of pipe condition.

Accordingly, Fig. 8 shows the mapping of corrosion of pipe specimens P1 to P3 with different immersion time duration of 30h, 472h, 912h, and 1080h. The areas of pipes subjected to high strains are shown in red color, indicating that the areas are under more severe corrosion. When specimens in P1 Group was monitored using fiber optic cables with different package thicknesses (outer diameter: 242 μm, 650 μm, and 900 μm), the results from different fiber optic cables show similar trends over time until 1080 h, which means that the coating thickness of fiber optic cable has little effect on the capability of measurement. However, for different deployment spacing, significant detection difference is noticed for various corrosion severity levels, which requires further investigation. For different space resolution, Fig. 8 cannot show clear the trends of the space resolution changes, requiring additional analysis.

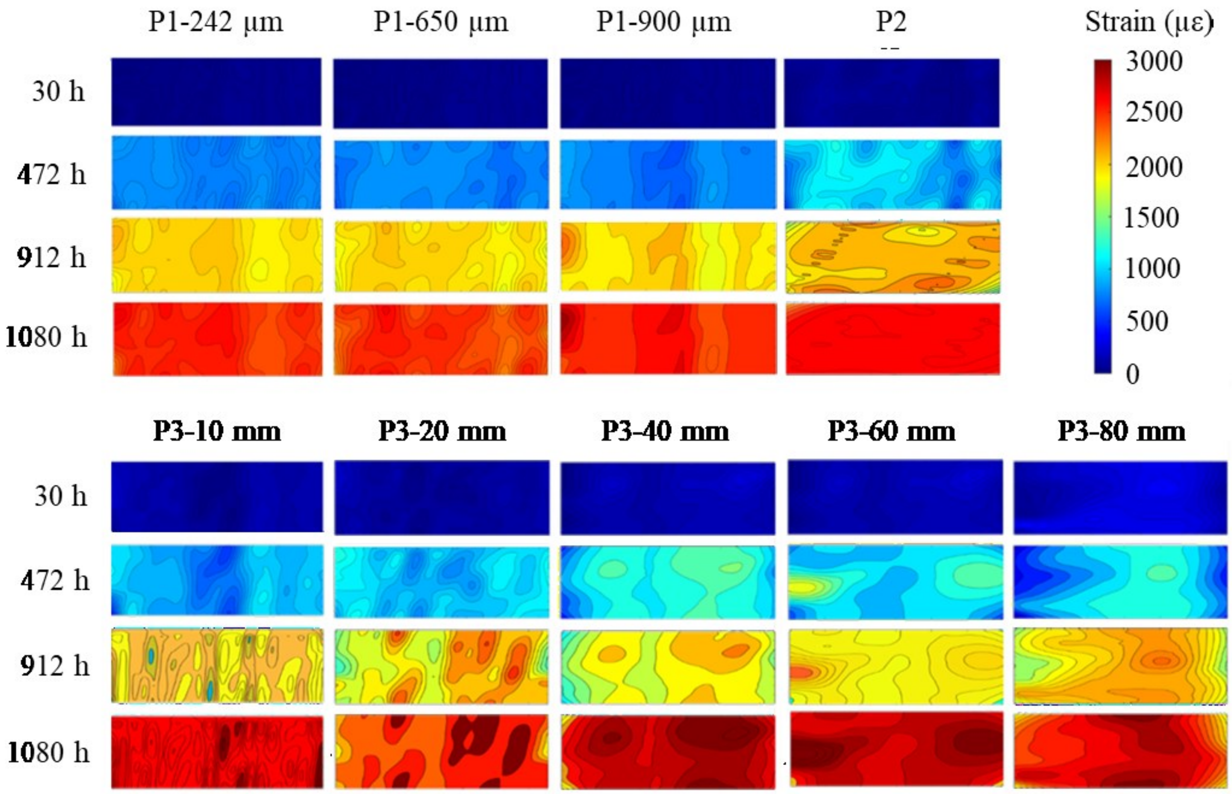

Fig. 8. Mapping of corrosion condition of specimens P1 to P3 at different times up to 1080 h.

To further investigate the influence of deployment spacing, Fig. 9(a) plots the monitored corrosion condition using different deployment spacing for 280h. It can be seen that as the spacing increased from 10 mm to 80 mm, the visualization results were highly changed, indicating that visualization was sensitive to the deployment spacing. The changes can be attributed to the uneven corrosion of the pipe. Coarse deployment of fiber optic cable may miss corrosion information.

For the effect of spatial resolution of strain distribution, Fig. 9(b) shows the monitored corrosion condition using different spatial resolutions for 280h. As the spatial resolution changed from 0.65 mm to 2.6 mm, there was no obvious difference in the images. As the spatial resolution further changed from 2.6 mm to 10.4 mm, obvious difference in the images could be observed; as the spatial resolution changed from 10.4 mm to 20.8 mm, the corrosion distribution could not be reasonably assessed, indicating that the spatial resolution had a significantly effect on visualization of corrosion.

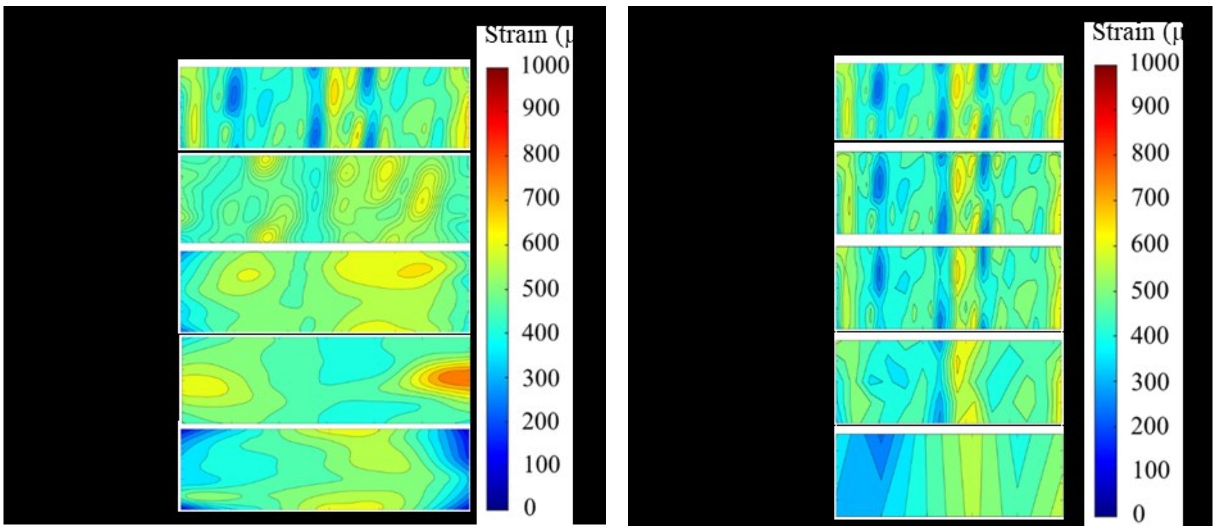

(a) (b)

Fig. 9. Corrosion condition of: (a) the P3 specimens at 280 h; and (b) the P2 specimens at 280 h.

4.4. Quantification

4.4.1. Mass loss evaluation

Mass loss evaluation is a common method used to evaluate corrosion of pipelines, as described in references [61, 62]. A reference sample of a pipe under consideration is prepared and placed near the pipe under corrosion. The mass loss of reference sample is measured to evaluate the mass loss of the pipe, assuming that the sample is subjected to the same corrosion rate as the pipe.

This study used short pipes as reference samples for mass loss evaluation, as shown in Fig. 10(a). The reference pipes measured 60 mm in length, and their two ends were sealed using plastic corks to prevent ingress of sodium chloride. Before the corrosion test, the reference pipes were cleaned, and the initial mass was measured using a high-precision microbalance (model: Mettler-Toledo Balance ME204E, USA), as shown in Fig. 10(b). The readability of the high-precision microbalance was 0.1 mg. Then, the reference pipes were immersed in the same sodium chloride solution as the test pipes with distributed sensors. Every 12 hours, one reference pipe was taken out of the solution to evaluate the mass loss, so the corrosion condition of pipes was assessed over time. Before mass measurement, the reference pipe was immersed in a vinegar acid (concentration: 45% by mass) for 6 h to remove corrosion products from the surface [63], as shown in Fig. 10(c). Then, the reference pipe was rinsed under running water. Next, it was placed in an oven at 70 °C for 15 min to get dried. After the reference pipe was cooled in air to room temperature, its mass was measured again using the balance. The mass of the reference sample was compared with its initial mass, and the mass difference is the mass loss (Δm) due to corrosion.

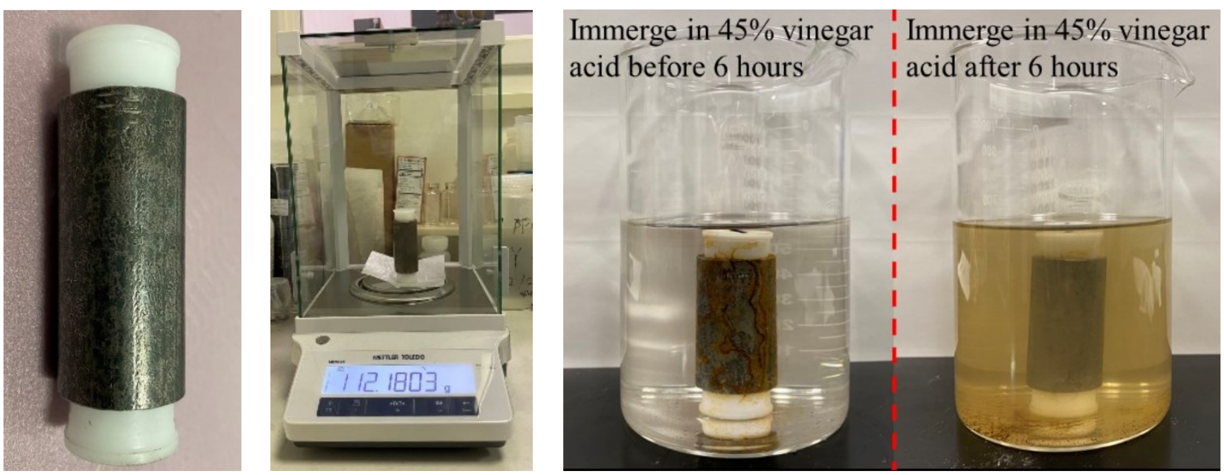

(a) (b) (c)

Fig. 10. Evaluation of mass loss: (a) reference pipe; (b) high-precision microbalance; and (c) reference pipe in a vinegar acid solution for removing surface rust.

4.4.2. Pipe corrosion model

Fig. 11 depicts a meso-scale model of steel pipe under corrosion. The pipe is instrumented with a fiber optic cable that is spirally winded on the surface. Due to symmetry, only a half of the cross section of pipe is shown. Since the fiber optic cable is winded on the surface of the pipe, the cut section of the cable has an ellipse shape in an arbitrary section perpendicular to the pipe length. The uncorroded section of the pipe is shown in orange color; the corrosion products (rust) that grow on the surface of the steel is shown in red color; the buffer of the fiber optic cable is shown in green color; and the fiber core is shown in white color. The rust is porous and has a larger volume than the steel, thus exerting pressure to the fiber optic cable. The pressure causes expansion of the fiber optic cable, and thus results in tensile strains in the fiber optic cable. Therefore, the strain change in the fiber optic cable reflects the corrosion process of the pipe.

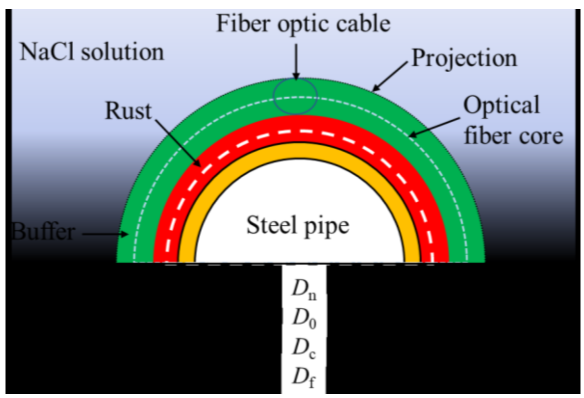

Fig. 11. Meso-scale corrosion model of a steel pipe with a fiber optic cable on the surface.

To derive formulae for evaluating mass loss due to corrosion using the distributed fiber sensors, the following assumptions are adopted including:

(1) The diameter of fiber optic cable does not affect the strain measurement because the diameter of the fiber optic cable is approximately 3.5% the diameter of the pipe. In real practices, the diameter of pipe is even larger, so the relative size of the fiber optic cable is small.

(2) All pipe corrosion products remain on the pipe surface. When pipes are embedded in soil or exposed to air, most corrosion products will stay on the pipe surface. Only a small amount of rust was transported to the solution, as shown in Fig. 5.

(3) The cross section of the pipe is circular throughout the corrosion process.

As shown in Fig. 11, the outer diameter of the pipe is D_0 (D_0 = 25.4 mm) before corrosion and D_n after corrosion, the diameter including the rust layer is D_c, and the diameter including the rust layer and a half thickness of fiber optic cable is D_f. Thus, the mass loss of the pipe (Δm) due to corrosion can be expressed as:

$$\Delta m = \frac{1}{4}\pi\left({D_0}^2 - {D_n}^2\right)\rho L \tag{4}$$

in which, L (L = 600 mm in this study) is he pipe length subjected to corrosion, ρ (ρ = 7850 kg/m^3 in this study) is the density of pipe material, k is the volume expansion coefficient of the rust.

The diameter of the pipe after corrosion can be expressed as:

$$D_n = \sqrt{\left({D_0}^2 - \frac{4\Delta m}{\pi\rho L}\right)} \tag{5}$$

According to the definition of strain, the tension strain along the fiber optic cable in the monitored pipe length (ε) can be expressed as:

$$\varepsilon = \frac{\pi(D_c - D_0)}{\pi D_0} = \frac{D_c - D_0}{D_0} \tag{6}$$

The volume of rust (V_r) and the volume of corroded pipeline (V_p) can then be estimated as:

$$V_r = \frac{1}{4}\pi\left({D_c}^2 - {D_n}^2\right)L \tag{7}$$

$$V_p = \frac{1}{4}\pi\left({D_0}^2 - {D_n}^2\right)L \tag{8}$$

The volume expansion coefficient of the rust can be determined as:

$$k = \frac{V_r}{V_p} = \frac{{D_c}^2 - {D_n}^2}{{D_0}^2 - {D_n}^2} \tag{9}$$

With Equations (5) and (6), Equation (4) can be rewritten as:

$$\Delta m = \frac{\pi\rho L{D_0}^2}{4(k-1)}\left(2\varepsilon + \varepsilon^2\right) \tag{10}$$

According to reference [48], the volume expansion coefficient of rust is a constant and is approximately equal to $k = 2$ for general corrosion. Thus, by assuming $k = 2$, Equation (10) can be rewritten as:

$$\Delta m \approx \frac{\pi \rho L {D_0}^2}{4}(2\varepsilon + \varepsilon^2) \tag{11}$$

Equation (11) describes the relationship between the mass loss of the pipe and the strain measured from the distributed sensor. In other words, once the strain distribution is measured from the distributed sensor, the mass loss of the pipe can be estimated using Equation (11). Accordingly, Figs. 12 (a-d) plot the estimated mass loss results of the tested pipes obtained from the monitored strains using the distributed fiber optic sensors for P0 to P3 Groups, respectively.

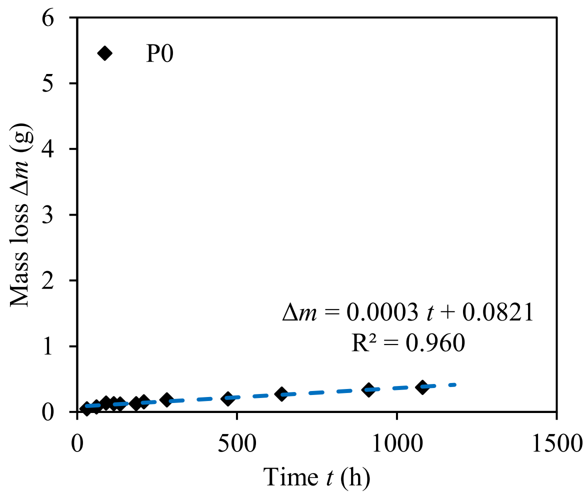

(a)

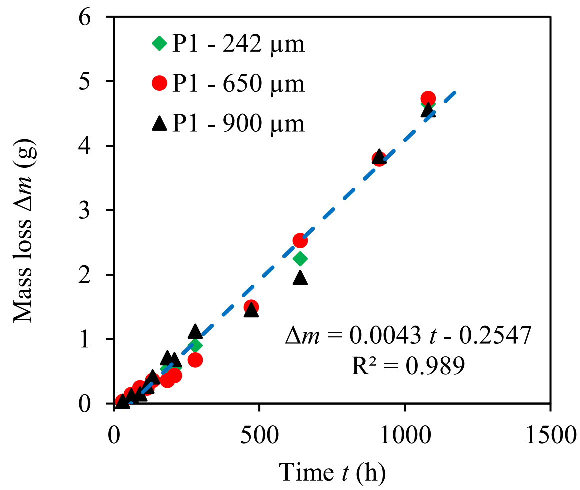

(b)

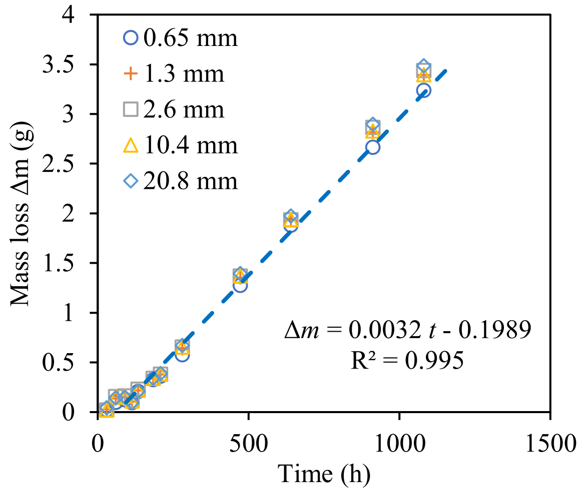

(c)

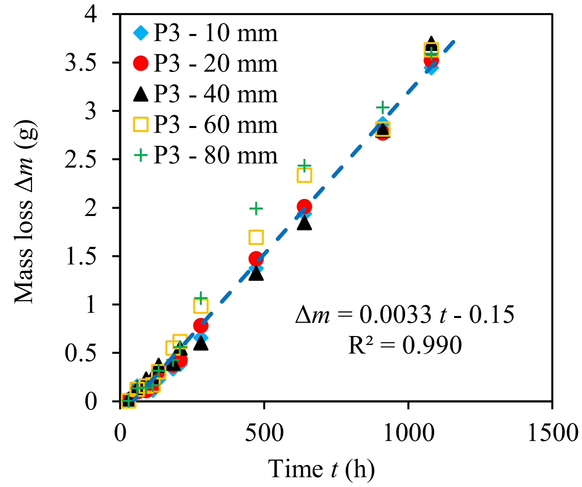

(d)

Fig. 12. Calculation results of mass loss of the pipe specimens: (a) P0; (b) P1; (c) P2; and (d) P3.

4.4.3. Calibration of corrosion expansion coefficient

To validate the mass loss measurements using the distributed optic fiber sensors, Fig. 13(a) compares the estimated mass loss of pipes (average value of P1, P2 and P3) against the measured mass loss using the high-precision microbalance as a reference. The data are fit using a linear equation through a regression analysis. The obtained coefficient of determination (R^2) is 0.994, indicating a good correlation. However, the slope of the fitting line is 1.799, meaning that there is a factor between the estimated mass loss using the distributed fiber optic sensors and the reference mass loss using microbalance. The factor can be attributed to the assumed value of k in Equation (13).

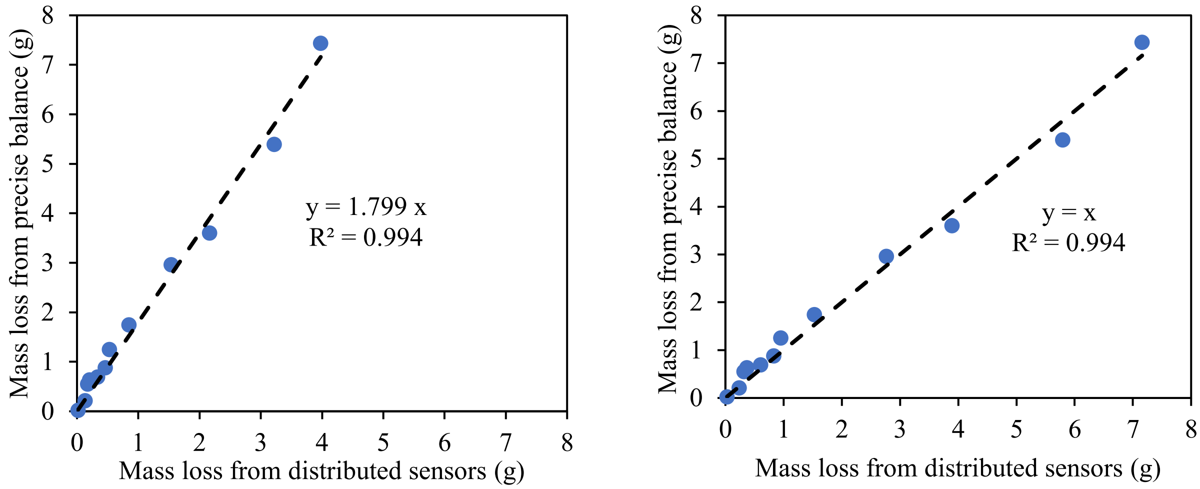

(a) (b)

Fig. 13. Comparison of measured and calculated mass loss of pipes when: (a) $k = 2$; (b) $k = 1.556$.

According to the slope of 1.799 in Fig. 13(a), the k value needs to be revised to $k = 1.556$ for the specific laboratory tests performed in this paper. Accordingly, Equation (11) can then be rewritten as Equation (12) using $k = 1.556$ as:

$$\Delta m \approx \frac{\pi \rho L {D_0}^2}{2.224}(2\varepsilon + \varepsilon^2) \tag{12}$$

By applying Equation (12), the mass loss is re-estimated and plotted in Fig. 13(b). The slope changed to 1.000, indicating that the proposed calibration method could provide reasonable evaluation of the mass loss of the pipe under corrosion.

4.4.4. Accuracy

With the corrosion assessment described using the mass loss of pipe (Δm) measured from the distributed sensors and high-precision microbalance, respectively, measurement error is defined based on mean absolute deviation [64], as described in Equation (13) below:

$$\text{Error} = \frac{1}{n}\sum_{i=1}^{n}\sqrt{\left(\Delta m_{\text{calculating},i} - \Delta m_{\text{fitting},i}\right)^2} \tag{13}$$

where n is the total number of data points; $\Delta m_{\text{calculating},i}$ is mass loss calculated using Equation (12) based on the measurement of strain distribution from the distributed sensor; and $\Delta m_{\mathrm{fitting},i}$ is mass loss determined from the linear fitting as shown in Fig. 13(b).

Fig. 14 shows the effects of coating thickness, spatial resolution, and deployment spacing on the accuracy of the proposed method for corrosion assessment. Fig. 14(a) shows the effect of coating thicknesses. As the coating thickness increased from 242 μm to 900 μm, there is only slight changes of error within 5%, meaning that the coating thickness does not significantly affect the accuracy. Therefore, fiber optic cables with a thick coating can be used to enhance the mechanical strength. Fig. 14(b) shows the effect of spatial resolution on the measurement error. It can be seen that as the spatial resolution changed from 0.65 mm to 20.8 mm, the error was approximately linearly increased from 0.110 g to 0.294 g, indicating that a fine spatial resolution benefits the measurement. Fig. 14(c) shows the effect of deployment spacing on measurement error. As the deployment spacing increased from 10 mm to 80 mm, the error was approximately linearly increased from 0.107 g to 0.343 g, indicating that a fine spacing could benefit the measurement.

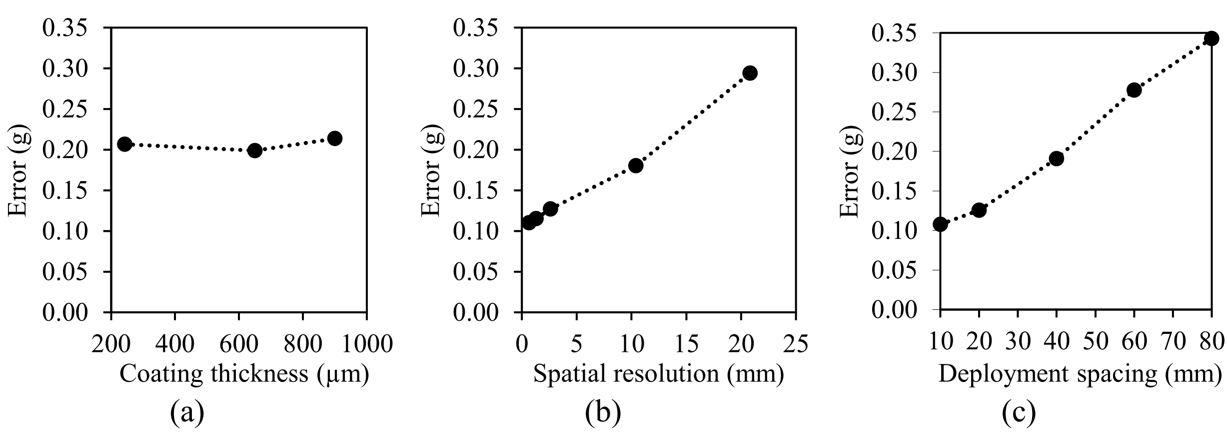

Fig. 14. Evaluation of measurement accuracy of mass loss due to corrosion under different: (a) coating thicknesses; (b) spatial resolutions; and (c) deployment spacings.

While the measured strain distributions slightly changed with the coating thickness, the spatial resolution and deployment spacing showed significant effects on the contours of corrosion and quantification of mass loss. It is recommended to use the following parameters for pipeline with an outer diameter of 25.4 mm as coating thickness of 900 μm, spatial resolution of 10.4 mm, and deployment spacing of 40 mm. Further research is needed for pipes with larger diameters.

4.5. Corrosion Warning

The mass loss of pipeline can be used to estimate the average corrosion rate (*CR in* mm/y = millimeter per year), as shown in Equation (14) [65]:

$$CR = \frac{\Delta m \times 365 \times 1000}{ATD} \tag{14}$$

where Δm is the mass loss (g); A is the initial exposed surface area (mm^2); T is exposure time (days); and D is density of metal (g/cm^3).

According to NACE SP0775-2018 [65], the average corrosion rate is "low" when *CR* is less than 0.025 mm/y; the average corrosion rate is "moderate" when *CR* is between 0.025 mm/y and 0.12 mm/y; the average corrosion rate is "high" when *CR* is between 0.12 mm/y and 0.25 mm/y; the average corrosion rate is "severe" when *CR* is larger than 0.25 mm/y. Fig. 18 plots the change of *CR* over time. After the pipe was exposed to the sodium chloride solution for 3 days, the value of *CR* exceeded 0.25 mm/y, indicating a "severe" corrosion. Thus, a corrosion warning could be issued.

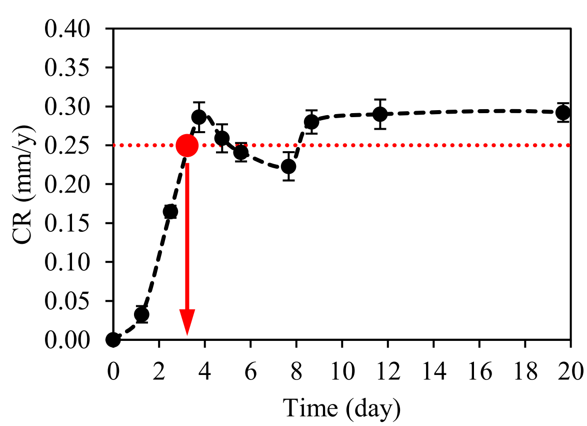

Fig. 15. Warning of pipeline corrosion condition based on the threshold of corrosion rate (CR).

5. Conclusions and Future Work

This paper introduces a real-time distributed pipeline corrosion monitoring method for detecting, locating, visualizing, and quantifying corrosion of pipeline using a single-mode telecommunication-grade fiber optic cable as a distributed fiber optic sensor. Laboratory accelerated corrosion experiments of steel pipes instrumented with different distributed sensors were conducted to investigate the effects of sensor package thickness, deployment pattern, and spatial resolution on corrosion assessment. An analytical model was developed and presented to correlate the measured strains with the mass loss of pipe under corrosion and utilized for quantification of corrosion. A threshold-based corrosion warning method is proposed for the pipeline corrosion management. The experimental results indicate that the developed method is promising for the real-time monitoring of pipeline corrosion without any influence on normal operation of pipeline.

Based on the above investigations, the following findings can be drawn:

- Corrosion of pipeline can induce strain change in distributed fiber optic sensor deployed on the surface of pipeline. As corrosion is developed, the tensile strain in distributed fiber optic sensor is increased. The strains measured from distributed fiber optic sensor can be used to detect corrosion on pipes. Strain distribution along a distributed fiber optic sensor can be used to locate corrosion on the pipe. With the correlation between distributed sensor length and position on the pipe, the strains measured from distributed fiber optic sensor can be used to locate and visualize corrosion on pipes.
- The proposed meso-scale analytical model can be used to describe the dimensional changes in the course of pipe corrosion and elucidate the mechanisms of monitoring pipe

corrosion using the distributed sensor. With the model, the strain measured from the distributed sensor can be used to quantify the mass loss of pipe due to corrosion. With the measurement results of mass loss of pipes, the rust expansion coefficient in the analytical model could be calibrated and enable reasonable predictions of mass loss using the strains measured from the distributed sensor. It is recommended to use 1.556 as the rust expansion coefficient (k) in future research and applications. Based on the capability of quantifying pipe corrosion, corrosion warning can be provided by the threshold of corrosion rate.

- The strain measurement and corrosion assessment results are dependent on the coating thickness, spatial resolution, and deployment spacing of the distributed sensor. While the measured strain distributions slightly changed with the coating thickness, the spatial resolution and deployment spacing showed significant effects on the contours of corrosion and quantification of mass loss. It is recommended to use the following indexes for pipelines with 25.4-mm outer diameter as coating thickness of 900 μm, spatial resolution of 10.4 mm, and deployment spacing of 40 mm.

Based on this paper, the following opportunities for future research are identified:

- In this paper, the pipe specimens were placed in sodium chloride solution to accelerate the corrosion reactions. However, the corrosion behavior could be different from the corrosion of pipes exposed to air or soil. Further research is needed to test the performance of the proposed method and calibrate the rust expansion coefficient.
- In real-life applications, the package of fiber optic cables and the adhesives used to install the fiber optic cables are subjected to degradation, thus compromising the service life of the distributed sensor. Further research is needed to investigate potential sensor degradation under realistic environmental conditions and plausible methods to improve

the durability.

- This study was focused on laboratory research and development using pipes with limited length and diameter. The performance of the proposed technology in real-life applications of large pipes remain unclear. Further research needs to be conducted to evaluate the performance and constructability of the proposed method. A life cycle cost assessment is needed to understand the economic impact of the distributed fiber optic sensors on intelligent management of pipelines.

Acknowledgement

This research was funded by the U.S. Department of Transportation through PHMSA [grant number: 693JK31950008CAAP, PI: Bao] and partially by National Science Foundation Grant #: CMMI-1750316 (PI: Huang). The contents of this paper reflect the views of the authors, and do not necessarily reflect the views of the sponsors.

References

[1] Pipeline and Hazardous Materials Safety Administration (PHMSA). "Annual report mileage for hazardous liquid or carbon dioxide systems." https://www.phmsa.dot.gov/data-and-statistics/pipeline/annual-report-mileage-hazardous-liquid-or-carbon-dioxide-systems. Accessed on March 30, 2021.

[2] Wright, R. F., Lu, P., Devkota, J., Lu, F., Ziomek-Moroz, M., and Ohodnicki, P. R. (2019). "Corrosion sensors for structural health monitoring of oil and natural gas infrastructure: A review." *Sensors*, 19(18), p.3964. https://doi.org/10.3390/s19183964

[3] Wright, R. F., Brand, E. R., Ziomek-Moroz, M., Tylczak, J. H., and Ohodnicki Jr, P. R. (2018). "Effect of HCO_3^- on electrochemical kinetics of carbon steel corrosion in CO_2-saturated brines." *Electrochimica Acta*, 290, pp.626-638. https://doi.org/10.1016/j.electacta.2018.09.114

[4] Fan, L., Tan, X., Zhang, Q., Meng, W., Chen, G., and Bao, Y. (2020). "Monitoring corrosion of steel bars in reinforced concrete based on helix strains measured from a distributed fiber optic sensor." *Engineering Structures*, 204, p.110039. https://doi.org/10.1016/j.engstruct.2019.110039

[5] U.S. National Association of Corrosion Engineers (NACE). "Pipelines and underground systems." https://www.nace.org/resources/industries-nace-serves/pipelines-underground-systems. Accessed on March 30, 2021.

[6] Pipeline and Hazardous Materials Safety Administration (PHMSA). "Fact Sheet: Corrosion." https://primis.phmsa.dot.gov/comm/FactSheets/FSCorrosion.htm?nocache=9090. Accessed on March 30, 2021.

[7] Kuprewicz, R. B. (2004). "Pipeline integrity and direct assessment a layman's perspective." *Pipeline Safety Trust*, p.7. http://pstrust.org/docs/direct_assessment.pdf. Accessed on March 30, 2021.

[8] Fessler, R. R. (2008). "Pipeline corrosion: Final report." *Pipeline and Hazardous Materials Safety Administration,* https://www.phmsa.dot.gov/sites/phmsa.dot.gov/files/docs/technical-resources/pipeline/gas-distribution-integrity-management/65996/finalreportpipelinecorrosion.pdf. Accessed on March 10, 2021.

[9] Cahill, J. (2019). "Continuously monitoring for pipeline corrosion." *Industry, Oil & Gas*, https://www.emersonautomationexperts.com/2019/industry/oil-gas/continuously-monitoring-pipeline-corrosion/. Accessed on March 30, 2021.

[10] Vanaei, H., Eslami, A., and Egbewande, A. (2017). "A review on pipeline corrosion, in-line inspection (ILI), and corrosion growth rate models." *International Journal of Pressure Vessels and Piping*, 149, pp.43-54. https://doi.org/10.1016/j.ijpvp.2016.11.007

[11] Gloria, N., Areiza, M., Miranda, I., and Rebello, J. (2009). "Development of a magnetic sensor for detection and sizing of internal pipeline corrosion defects." *NDT & E International*, 42(8), pp.669-677. https://doi.org/10.1016/j.ndteint.2009.06.009

[12] Kim, D., Udpa, L., and Udpa, S. (2004). "Remote field eddy current testing for detection of stress corrosion cracks in gas transmission pipelines." *Materials Letters*, 58(15), pp.2102-2104. https://doi.org/10.1016/j.matlet.2004.01.006

[13] Lei, H., Huang, Z., Liang, W., Mao, Y., and Que, P. (2009). "Ultrasonic pig for submarine oil pipeline corrosion inspection." *Russian Journal of Nondestructive Testing*, 45(4), pp.285-291. https://doi.org/10.1134/S106183090904010X

[14] Pollock, A. A. (1986). "Acoustic emission capabilities and applications in monitoring corrosion." *Corrosion Monitoring in Industrial Plants Using Nondestructive Testing and Electrochemical Methods*, ASTM International, pp.30-42. https://doi.org/10.1520/STP17435S

[15] Schmidt, R. (2004). "Unpiggable pipelines–What a challenge for in-line inspection!" *Pigging Products and Services Association (PPSA)* https://ppsa-online.com/papers/2004-Aberdeen-7-Schmidt.pdf. Accessed on March 30, 2021.

[16] Zhang, X., Jiang, Z. H., Yao, Z. P., Song, Y., and Wu, Z. D. (2009). "Effects of scan rate on the potentiodynamic polarization curve obtained to determine the Tafel slopes and corrosion current density." *Corrosion Science*, 51(3), pp.581-587. https://doi.org/10.1016/j.corsci.2008.12.005

[17] Wandelt, K. (2018). *Encyclopedia of Interfacial Chemistry: Surface Science and Electrochemistry*. https://www.sciencedirect.com/referencework/9780128098943/encyclopedia-of-interfacial-chemistry.

[18] Roberge, P. R. (2019). *Handbook of Corrosion Engineering*, McGraw-Hill Education. https://www.accessengineeringlibrary.com/content/book/9781260116977

[19] "Linear polarization resistance and corrosion rate: Theory and background." https://pineresearch.com/shop/wp-content/uploads/sites/2/2016/07/DRA10086-Linear-Polarization-and-Corrosion-Rate-Overview-REV002.pdf. Accessed on March 30, 2021.

[20] Mansfeld, F. (1976). "The effect of uncompensated IR-drop on polarization resistance measurements." *Corrosion*, 32(4), pp.143-146. https://doi.org/10.1016/0010-938X(78)90013-6

[21] Angst, U., and Büchler, M. (2015). "On the applicability of the Stern–Geary relationship to determine instantaneous corrosion rates in macro-cell corrosion." *Materials and Corrosion*, 66(10), pp.1017-1028. https://doi.org/10.1002/maco.201407997

[22] Papavinasam, S. (2013). *Corrosion Control in the Oil and Gas Industry*, Elsevier. https://www.sciencedirect.com/book/9780123970220/corrosion-control-in-the-oil-and-gas-industry

[23] Li, S., Kim, Y.-G., Jung, S., Song, H.-S., and Lee, S.-M. (2007). "Application of steel thin film electrical resistance sensor for in situ corrosion monitoring." *Sensors and Actuators B: Chemical*, 120(2), pp.368-377. https://doi.org/10.1016/j.snb.2006.02.029

[24] Sonyok, D., Zhang, B., and Zhang, J. (2008). "Applications of non-destructive evaluation (NDE) in pipeline inspection." *Pipelines 2008: Pipeline Asset Management: Maximizing Performance of our Pipeline Infrastructure*, pp.1-10. https://doi.org/10.1061/40994(321)105

[25] Fajardo, S., García-Galvan, F. R., Barranco, V., Galvan, J. C., and Batlle, S. F. (2018). "A critical review of the application of electrochemical techniques for studying corrosion of mg and mg alloys: Opportunities and challenges." *Magnesium Alloys-Selected Issue*. https://doi.org/10.5772/intechopen.79497

[26] Adegboye, M. A., Fung, W.-K., and Karnik, A. (2019). "Recent advances in pipeline monitoring and oil leakage detection technologies: Principles and approaches." *Sensors*, 19(11), p.2548. https://doi.org/10.3390/s19112548

[27] Kim, H. J. (2016). "Investigation on the vibrating wire strain gauges for the evaluation of pipeline safety in extreme cold region." *The Journal of Engineering Geology*, 26(4), pp.583-591. https://doi.org/10.9720/kseg.2016.4.583

[28] Chapetti, M., Otegui, J., and Motylicki, J. (2002). "Fatigue assessment of an electrical resistance welded oil pipeline." *International Journal of Fatigue*, 24(1), pp.21-28. https://doi.org/10.1016/S0142-1123(01)00111-6

[29] Barrias, A., Casas, J. R., and Villalba, S. (2016). "A review of distributed optical fiber sensors for civil engineering applications." *Sensors*, 16(5), p.748. https://doi.org/doi.org/10.3390/s16050748

[30] Cherukupalli, S., and Anders, G. J. (2019). *Distributed Fiber Optic Sensing and Dynamic Rating of Power Cables*, John Wiley & Sons. https://ieeexplore.ieee.org/servlet/opac?bknumber=8889853

[31] Bao, Y., Huang, Y., Hoehler, M. S., and Chen, G. (2019). "Review of fiber optic sensors for structural fire engineering." *Sensors*, 19(4), p.877. https://doi.org/10.3390/s19040877

[32] Bao, Y., Valipour, M., Meng, W., Khayat, K. H., and Chen, G. (2017). "Distributed fiber optic sensor-enhanced detection and prediction of shrinkage-induced delamination of ultra-high-performance concrete overlay." *Smart Materials and Structures*, 26(8), 085009. https://doi.org/10.1088/1361-665X/aa71f4

[33] Bao, Y. (2017). "Novel applications of pulse pre-pump Brillouin optical time domain analysis for behavior evaluation of structures under thermal and mechanical loading." *Doctoral*

Dissertations.https://scholarsmine.mst.edu/cgi/viewcontent.cgi?article=3585&context=doctoral_dissertations

[34] Vahdati, N., Wang, X., Shiryayev, O., Rostron, P. and Yap, F.F., (2020). "External corrosion detection of oil pipelines using fiber optics." *Sensors*, 20(3), p.684. https://doi.org/10.3390/s20030684

[35] Wei, H., Liao, K., Zhao, X., Kong, X., Zhang, P. and Sun, C., (2019). "Low-coherent fiber-optic interferometry for in situ monitoring the corrosion-induced expansion of pre-stressed concrete cylinder pipes." *Structural Health Monitoring*, 18(5-6), pp.1862-1873. https://doi.org/10.1177/1475921719826360

[36] Lu, P., Wright, R.F., Ziomek-Moroz, M., Buric, M.P., Zandhuis, P. and Ohodnicki, P.R., (2018). "A multifunctional fiber optic sensor for internal corrosion monitoring in natural gas transmission pipelines." *NACE International Corrosion Conference Proceedings*, pp.1-12. NACE. https://search.proquest.com/docview/2463181656/fulltextPDF/CF8E54A96DAD46C1PQ/1?accountid=14052

[37] Li, W., Liu, T. and Xiang, H., Leakage detection of water pipelines based on active thermometry and FBG based quasi-distributed fiber optic temperature sensing. *Journal of Intelligent Material Systems and Structures*, p.1045389X20987002. https://doi.org/10.1177/1045389X20987002

[38] Feng, X., Han, Y., Wang, Z. and Liu, H., (2018). "Structural performance monitoring of buried pipelines using distributed fiber optic sensors." *Journal of Civil Structural Health Monitoring*, 8(3), pp.509-516. https://doi.org/10.1007/s13349-018-0286-3

[39] Ren, L., Jiang, T., Jia, Z.G., Li, D.S., Yuan, C.L. and Li, H.N., (2018). "Pipeline corrosion and leakage monitoring based on the distributed optical fiber sensing technology." *Measurement*, 122, pp.57-65. https://doi.org/10.1016/j.measurement.2018.03.018

[40] Ren, L., Jiang, T., Li, D.S., Zhang, P., Li, H.N. and Song, G.B., (2017). "A method of pipeline corrosion detection based on hoop-strain monitoring technology." *Structural Control and Health Monitoring*, 24(6), p.e1931. https://doi.org/10.1002/stc.1931

[41] Jiang, T., Ren, L., Jia, Z.G., Li, D.S. and Li, H.N., (2017). "Pipeline internal corrosion monitoring based on distributed strain measurement technique." *Structural Control and Health Monitoring*, 24(11), p.e2016. https://doi.org/10.1002/stc.2016

[42] Wright, R.F., Ziomek-Moroz, M. and Ohodnicki Jr, P.R., (2018). "Fe Thin Film Coated Optics for Monitoring Internal Corrosion in Natural Gas Pipelines." *NACE International Corrosion Conference Proceedings*, pp.1-13. National Association of Corrosion Engineers. https://search.proquest.com/docview/2463178009?pq-origsite=gscholar&fromopenview=true

[43] Wright, R.F., Badar, M., Egbu, J.C., Lu, P., Buric, M. and Ohodnicki Jr, P.R., (2019). "Fully distributed optical fiber sensor for water and humidity monitoring." *Fiber Optic Sensors and Applications XVI*, 11000, p.1100007. International Society for Optics and Photonics. https://doi.org/10.1117/12.2519239

[44] Wright, R.F., Egbu, J., Lu, P., Buric, M., Ziomek-Moroz, M. and Ohodnicki Jr, P.R., (2019). "Electrolessly Coated Optical Fibers for Distributed Corrosion Monitoring." *NACE International Corrosion Conference Proceedings*, pp.1-12. National Association of Corrosion Engineers. https://search.proquest.com/docview/2463696489?pq-origsite=gscholar&fromopenview=true

[45] Fan, L., Bao, Y., Meng, W., and Chen, G. (2019). "In-situ monitoring of corrosion-induced expansion and mass loss of steel bar in steel fiber reinforced concrete using a distributed fiber optic

sensor." *Composites Part B: Engineering*, 165, pp.679-689. https://doi.org/10.1016/j.compositesb.2019.02.051

[46] Almahmoud, S., Shiryayev, O., Vahdati, N. and Rostron, P., (2018). "Detection of internal metal loss in steel pipes and storage tanks via magnetic-based fiber optic sensor." *Sensors*, 18(3), p.815. https://doi.org/10.3390/s18030815

[47] Almahmoud, S., Shiryayev, O., Vahdati, N. and Rostron, P., (2017). "Feasibility of magnetic fiber-optic based corrosion sensor." *Sensors and Smart Structures Technologies for Civil, Mechanical, and Aerospace Systems 2017*, 10168, p.101681M. International Society for Optics and Photonics. https://doi.org/10.1117/12.2260882

[48] Shiryayev, O., Cullin, M. and Srinivasan, R., (2021). "On the development of an improved magnetic-based corrosion sensor." *Sensors and Smart Structures Technologies for Civil, Mechanical, and Aerospace Systems 2021*, 11591, p.115911M. International Society for Optics and Photonics. https://doi.org/10.1117/12.2583312

[49] Bao, X., and Chen, L. (2012). "Recent progress in distributed fiber optic sensors." *Sensors*, 12(7), pp.8601-8639. https://doi.org/10.3390/s120708601

[50] Fan, L., Bao, Y., and Chen, G. (2018). "Feasibility of distributed fiber optic sensor for corrosion monitoring of steel bars in reinforced concrete." *Sensors*, 18(11), p.3722. https://doi.org/10.3390/s18113722

[51] Zhao, X., Gong, P., Qiao, G., Lu, J., Lv, X., and Ou, J. (2011). "Brillouin corrosion expansion sensors for steel reinforced concrete structures using a fiber optic coil winding method." *Sensors*, 11(11), pp.10798-10819. https://doi.org/10.3390/s111110798

[52] Casas, J., Villalba, S., and Villalba, V. (2014). "Management and safety of existing concrete structures via optical fiber distributed sensing." *Maintenance and Safety of Aging Infrastructure:*

Structures and Infrastructures Book Series; CRC Press: Boca Raton, FL, USA, 10, pp.217-245. https://doi.org/10.1201/b17073-9

[53] Palmieri, L., and Schenato, L. (2013). "Distributed optical fiber sensing based on Rayleigh scattering." *The Open Optics Journal*, 7(1). https://doi.org/10.2174/1874328501307010104

[54] Ding, Z., Wang, C., Liu, K., Jiang, J., Yang, D., Pan, G., Pu, Z., and Liu, T. (2018). "Distributed optical fiber sensors based on optical frequency domain reflectometry: A review." *Sensors*, 18(4), p.1072. https://doi.org/10.3390/s18041072

[55] Tan, X., Bao, Y., Zhang, Q., Nassif, H., and Chen, G. (2021). "Strain transfer effect in distributed fiber optic sensors under an arbitrary field." *Automation in Construction*, 124, p.103597. https://doi.org/10.1016/j.autcon.2021.103597

[56] Tan, X., and Bao, Y. (2021). "Measuring crack width using a distributed fiber optic sensor based on optical frequency domain reflectometry." *Measurement*, 172, p.108945. https://doi.org/10.1016/j.measurement.2020.108945

[57] Tan, X., Abu-Obeidah, A., Bao, Y., Nassif, H., and Nasreddine, W. (2021). "Measurement and visualization of strains and cracks in CFRP post-tensioned fiber reinforced concrete beams using distributed fiber optic sensors." *Automation in Construction*, 124, p.103604. https://doi.org/10.1016/j.autcon.2021.103604

[58] Gifford, D. K., Kreger, S. T., Sang, A. K., Froggatt, M. E., Duncan, R. G., Wolfe, M. S., and Soller, B. J. "Swept-wavelength interferometric interrogation of fiber Rayleigh scatter for distributed sensing applications." *Proc., Fiber Optic Sensors and Applications V*, International Society for Optics and Photonics, p.67700F. https://doi.org/10.1117/12.734931

[59] ASTM A733-16 (2016). *Standard Specification for Welded and Seamless Carbon Steel and Austenitic Stainless Steel Pipe Nipples*, ASTM International, West Conshohocken, PA. http://www.astm.org/cgi-bin/resolver.cgi?A733-16

[60] ASTM A269-15a (2019). *Standard Specification for Seamless and Welded Austenitic Stainless Steel Tubing for General Service*, ASTM International, West Conshohocken, PA. http://www.astm.org/cgi-bin/resolver.cgi?A269A269M-15a(2019)

[61] Palanisamy, K., Devabharathi, V., and Sundaram, N. M. (2014). "Corrosion inhibition studies of mild steel with carrier oil stabilized of iron oxide nanoparticles incorporated into a paint." *International Journal of ChemTech Research* 7(4), pp.1661-1664. http://sphinxsai.com/2015/ch_vol7_no4/1/(1661-1664)%20V7N4.pdf

[62] Usman, A. D., Victoria, A. F., and Okoro, L. N. (2015). "Weight loss corrosion study of some metals in acid medium." *Journal: Journal of Advances in Chemistry*, 11(2), pp.3434-3440. https://doi.org/10.24297/jac.v11i2.2211

[63] Kahyarian, A., Schumaker, A., Brown, B., and Nesic, S. (2017). "Acidic corrosion of mild steel in the presence of acetic acid: Mechanism and prediction." *Electrochimica Acta*, 258, pp.639-652. https://doi.org/10.1016/j.electacta.2017.11.109

[64] Gentry, T. W., Wiliamowski, B. M., and Weatherford, L. R. (1995). "A comparison of traditional forecasting techniques and neural networks." *Intelligent Engineering Systems Through Artificial Neural Networks*, 5, pp.765-770. https://doi.org/10.1016/S2092-5212(11)80022-2

[65] NACE SP0775 (2018). *Preparation, Installation, Analysis, and Interpretation of Corrosion Coupons in Oilfield Operations*, NACE International Institute, Houston, Texas, USA. https://store.nace.org/sp0775-2013-formerly-rp0775-18854